Journal of Drug Delivery Science and Technology 31 (2016) 153–159

Contents lists available at ScienceDirect

Journal of Drug Delivery Science and Technology

journal homepage: www.elsevier.com/locate/jddst

Research paper

Synthesis and application of the MCM-41 and SBA-15 as matrices for in vitro efavirenz release study

R.A. Jesus [a], A.S. Rabelo [b], R.T. Figueiredo [b], L.C. Cides da Silva [c], I.C. Codentino [d], M.C.A. Fantini [e], G.L.B. Araújo [f], A.A.S. Araújo [b], M.E. Mesquita [a, *]

[a] Departamento de Química, Universidade Federal de Sergipe-UFS, Av. Marechal Rondon, s/n, Cidade Universitária, CEP 49100-000, São Cristóvão, SE, Brazil
[b] Departamento de Fisiologia, Universidade Federal de Sergipe-UFS, Av. Marechal Rondon, s/n, Cidade Universitária, CEP 49100-000, São Cristóvão, SE, Brazil
[c] Departamento de Química Fundamental, Instituto de Química, Universidade de São Paulo-USP, C.P. 66083, São Paulo, SP, Brazil
[d] Departamento de Física Aplicada, Instituto de Física, USP, CP 66318, 053-970, São Paulo, SP, Brazil
[e] Instituto de Pesquisas Energéticas e Nucleares – IPEN, Av. Prof. Lineu Prestes, 2242, CEP 05508-900, São Paulo, SP, Brazil
[f] Departamento de Farmácia, Faculdade de Ciências Farmacêuticas, Universidade de São Paulo, Av. Professor Lineu Prestes, 580, CEP 05508-000, São Paulo, SP, Brazil

ARTICLE INFO

Article history:
Received 5 August 2015
Received in revised form
1 November 2015
Accepted 28 November 2015
Available online 17 December 2015

Keywords:
Mesoporous
Controlled release
EFZ

ABSTRACT

The mesoporous materials in particular the Mobil Composition of Matter No. 41 (MCM-41) and Santa Barbara Amorphous-15 (SBA-15) are considered promising as devices for controlled drug release, because of properties such as hexagonal arrangement, high surface area and non-cytotoxic properties. The materials were synthesized under hydrothermal method and efavirenz (EFZ) was used for testing of controlled release. The material obtained was ordered and had high surface area even after of the incorporation of the drug. The test of the release was made with capsules and the reading was made by UV/Vis with the time interval during two hours to evaluation the efficiency of the dissolution profile of the drug.

1. Introduction

The introduction of highly active antiretroviral therapy (HAART) involving the use of drug combinations to treat of human immunodeficiency virus type 1 (HIV-1) infection has resulted in a significant reduction in the death rate from AIDS for patients receiving such treatment [1,2]. EFZ is a specific, non-nucleoside reverse transcriptase inhibitor (NNRTI) of HIV-1 [3,4]. EFZ has been found to be effective in many combination regimens for HIV treatment [5].

The administration of drugs by a drug delivery system provides advantages over conventional drug therapies because the drug is delivered locally rather than systemically. This minimizes harmful side effects [6,7]. For controlled release applications, it has been shown that silica is able to store and gradually release therapeutically relevant drugs like antibiotics, and others. Furthermore, silica is used to enhance the biocompatibility of several drug delivery systems, such as magnetic nanoparticles, biopolymers, and micelles [8].

The discovery of ordered mesoporous silicas (OMSs) opened new pathways for researchers of materials with well-defined porous structures and planning particle morphologies [9,10]. The first articles on OMSs were made to the MCM-41 by Mobil researchers in 1992, which has been prepared in the presence of cationic surfactants in basic media and it was used mesitylene (1,3,5-trimethyl benzene)as swelling agent [9,10]. Afterward, the use of triblock copolymers as templates opened an intensive research in this area of OMSs. The OMS SBA-15 [11,12], which possesses a hexagonal structure of cylindrical mesopores, interconnected by micropores randomly distributed (p6mm symmetry), was one of the first OMS prepared using triblock copolymer, in this case Pluronic P123 of BASF corporation; under acidic conditions from either tetraethyl orthosilicate (TEOS) or sodium silicate used as silica source.

The SBA-15 [11,12] is comparable to MCM-41 [9,10], however, in addition to the aforementioned interconnecting fine pores it exhibits larger pore diameters, and thicker walls; thus it presents a better hydrothermal and thermal stabilities than its similar, MCM-41 [13]. Recently, research has been focused on the application of OMSs based materials as a potential drug delivery system.

* Corresponding author.
E-mail address: mariaelianemesquita3@gmail.com (M.E. Mesquita).

http://dx.doi.org/10.1016/j.jddst.2015.11.008
1773-2247/

Mesoporous silica nanoparticles have high surface area, large pore volume, uniform porosity, and stable aqueous dispersion. Their excellent biocompatibility, in vivo biodegradability, and the capability to be functionalized with different organic groups make them attractive candidates for a wide range of biomedical purposes, such as controlled drug delivery [14].

2. Experimental

2.1. Materials

Silica (SiO_2), surfactant cetyltrimethylammonium bromide (CTMABr), tetra ethyl ortho silicate (TEOS), surfactant (Pluronic P123 123 from BASF) Triblock copolymer, ammonia fluoride (NH_4F) and Sodium lauryl sulfate (SLS) were from Sigma Aldrich. Sodium silicate (Na_2SiO_3) was obtained in the VETEC. Acetic acid ($C_2O_2H_4$) and hydrochloric acid (HCl) was obtained from Synth. EFZ was obtained in the Foundation for Science and Technology of Pernambuco (FACEPE).

2.2. Synthesis

2.2.1. Synthesis of silica MCM-41

The synthesis was carried outusing two solutions. The first solution was made dissolving 0.911 g of SiO_2, 0.705 g of Na_2SiO_3 in 8.4 mL of distilled water (H_2O) under stirring in a range temperature of 40–50 °C. The resulting mixture was stirred until complete homogeneity over a period of 2 h. The second solution consisted of dissolving 1.743 g of CTMABr in 8.3 mL distilled water with stirring at room temperature until complete homogeneity over a period of 30 min. Subsequently, the 1st solution was added to 2nd solution under vigorous stirring at room temperature for 30 min. The molar of gel composition used was: 1.0 CTMABr: 0.83 Na_2SiO_3: 0.31 SiO_2: 194 H_2O. The gel obtained was introduced into a stainless steel autoclave and heated at 100 °C in an oven for a period of 72 h, by controlling the pH of each gel 24 for 9–10 h with 5% $C_2O_2H_4$ until it reached stability. Finally, the precipitate was filtered out, washed with H_2O and dried at 25 °C and calcinated under nitrogen, which was afterwards switched to air, at 550 °C [15].

2.2.2. Synthesis of silica SBA-15

For the synthesis of SBA-15 from TEOS, 2.50 g of surfactante (P123, Pluronic 123 from BASF) triblock copolymer, 0,0312 g of NH_4F was added to 100 mL of 0.01 mol L^{-1} HCl solution and stirred for 1 h in room temperature. Next, 5.8 mL of TEOS was added in the mixture under stirring for 1 h in room temperature. The resulting mixture was stirred for 24 h at a temperature of 35 °C. The obtained gel was transferred to an Teflon®autoclave and heated in an oven to a temperature of 100 °C for 48 h. Finally, the precipitate was filtered out, washed with distilled water and dried at 25 °C and calcinated under nitrogen, which was afterwards switched to air, at 540 °C [16].

2.3. EFZ incorporation of the MCM-41 and SBA-15

The incorporation of the EFZ at MCM-41 and SBA-15 silica was taken in a 1:1 (w/w) mesoporous matrix: EFZ in dichloromethane under magnetic stirring system was then dried in a rota-evaporator.

2.4. Characterization

2.4.1. Small angle X-ray scattering (SAXS)

The SAXS measurements were performed with a Nanostar, Bruker, set-up operating at 1.2 kW. The wavelength of the X-ray beam of monochromatic CuK copper “alpha” was $\lambda = 0.15418$ nm. A filament in two dimensions Vantec detector was used to record the vector scatter q = (4psintheta)/lambda, where q is the vector scatter, q being half the scattering angle wave vector band used was 0.008 “angstrom” ^ − 1 < Q < 35 “angstrom” ^ − 1, 4 “pi” pi = 3.1416 and sin theta refers to experience diffraction of X-rays at low angles of the hexagonal structures with peaks at Bragg angles lambda = 2d(hkl)xsintheta(hkl).*(hkl) are the Miller indices. The intensity was recorded for 10 min. The focus point geometry was used and the system was collimated by slots. The assembly takes up a vacuum path and the sample chamber. The sample to detector distance (~640 mm) was chosen in order to record the intensity of the dispersion to values of Q ranging from 0.1 to 1 nm, 3.5 nm-1. The sample was placed between the mica discs of 20 mm diameter. The dispersion of the sample support was subtracted from the measured total intensities. All data were normalized and corrected for the effects of absorption.

2.4.2. Nitrogen sorption isotherms

N_2 sorption isotherms were measured at −196 °C, using nitrogen of 99.998% purity, on a Micromeritics ASAP 2010 volumetric sorption analyzer. Measurement was performed in the range of relative pressure from 10^{-6} to 0.99. Before the sorption measurement, the sample was outgassed at 200 °C in the port of the sorption analyzer. Specific surface area was evaluated using the Brunauer–Emmett–Teller method (BET). The total pore volume, V_{Pt} ($cm^3\ g^{-1}$), was estimated from the amount adsorbed at the relative pressure of 0.99 and the microporous volume, V_{mi} ($cm^3\ g^{-1}$), was calculated using the standard reduced adsorption data. Pore size distribution (PSD) was calculated using the Barret, Joyner e Halenda (BJH) algorithm with the relation between capillary condensation pressure and pore diameter established by [17].

2.4.3. High-Resolution Transmission Electronic Microscopy (HRTEM)

For HRTEM observation, the samples were studied using a microscope JEOL, model JEM 2100 (Cs 1.4 mm, resolution, point 0.25 nm, 0.14 nm grid) to 200 kV. The high-resolution images HRTEM were recorded on a slow-scan CCD (Gatan Orius SC1000). To prepare the samples, the samples were dispersed in isopropyl alcohol, sonicated for 5 min and put onto a carbon film deposited on a 400 mesh Cu grid [18].

2.4.4. Thermal analysis

Differential scanning calorimetry (DSC) curves were obtained in a DSC-50 cell (Shimadzu) using aluminium crucibles with about 2 mg of samples, under dynamic nitrogen atmosphere (50 mL·min^{-1}) and heating rate of 10 °C min^{-1} in the temperature range from 25 to 500 °C. The DSC cell was calibrated with indium (p.m. 156.6 °C; $\Delta H_{fus.} = 28.54\ J\ g^{-1}$) and zinc (p.m. 419.6 °C).

2.5. In vitro drug release study

The evaluation of in vitro drug release from MCM-41/EFZ and SBA-15/EFZ were performed using USP Apparatus 1 (Agilent Technologies – 708 – DS Dissolution Apparatus) in 900 mL of water with 1% SLS stirred at 37 ± 0.5 °C and 50 rpm; the dissolution medium and experimental conditions were selected according to the methodologies reported in the U.S. Food and Drug Administration database of dissolution methods for efavirenz capsules and the Brazilian official pharmacopoeia [19,20]. A powder sample equivalent to approximately 60 mg of the EFZ filled into capsules was tested. The accurately weighed capsules were placed in the basket, and processed for dissolution testing. Dissolution samples (3 mL) were withdrawn at regular intervals (0, 5, 10, 15, 20, 30, 45,

60, 75, 90) with no media replacement [21,22]. To obtain an infinity point, the basket speed was increased to 250 rpm at the end of the run for a sustained period of 30 min, after which time an additional sample was taken [23]. The samples were filtered immediately by 0.45 μm PVDF filter and the quantity of released EFZ was measured using a UV–vis spectrophotometer at the wavelength of 247 nm, by taking 3 mL samples at desired time intervals. Drug concentration was calculated using a calibration curve. Dissolution sampling-volume correction and data analysis and were carried out using the Excel add-in DDSolver program developed by Zhang and co-workers [24].

3. Results and discussion

3.1. Characterization

3.1.1. SAXS

Figs. 1 and 2 show the positions of the peaks are consistent with the structure of two-dimensional hexagonal symmetry type p6mm for the MCM-41 C (calcined) and SBA-15 C. Sample of the MCM-41 C, present four peaks well resolved, indexed in positions (100), (110), (200) and (210). The samples of SBA-15 C, present five peaks well resolved, indexed in positions (100), (110), (200), (210) and (300). The interplanar spacing [$d_{(hkl)}$] and the lattice parameter (a) were calculated for the (100) reflection. After encapsulation of the EFZ drug in the ordered mesoporous structures (MCM-41 and SBA-15) were not destroyed. The observed small decrease of the diffracted intensities of the EFZ drug in MCM-41 (Fig. 1) and EFZ in SBA-15 (Fig. 2) are attributed to the decrease of the electronic contrast between silica and mesoporous media. The peak (100) interplanar distance of MCM-41 samples did not show a significant change when comparing MCM-41 and MCM-41/EFZ, but for seems that the material swells after the drug encapsulation inside it.

This is an indicative that the EFZ is inside the mesoporous, moreover, it encapsulation promotes a swelling of the pores for the MCM-41. For the SBA-15 samples did not occur change significantly of the diffracted intensities and lattice parameters between (100) peaks of the SBA-15 samples (Fig. 2). After the encapsulation of EFZ inside of the SBA-15, the intensities decrease, as expected, but in small extension when compared to similar MCM-41 samples. In this case, for the SBA-15 samples, lattice parameters remained unchanged (Table 1). The data of interplanar spacing [$d_{(hkl)}$] and lattice parameters [a] are listed in Table 1.

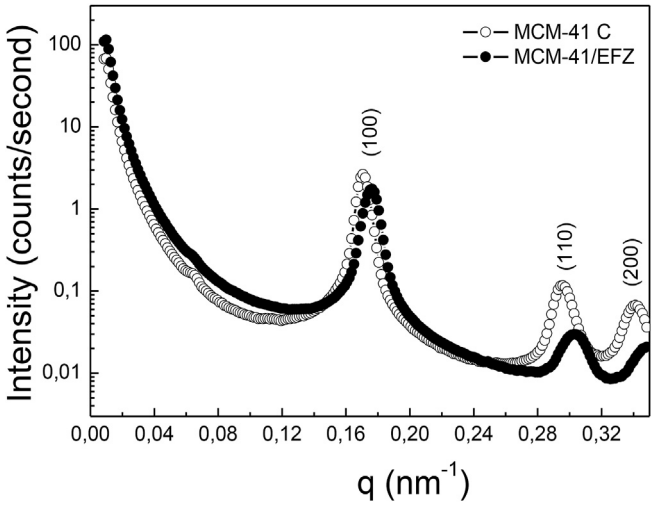

Fig. 1. Small angle X-ray scattering of ordered mesoporous silica MCM-41 sample.

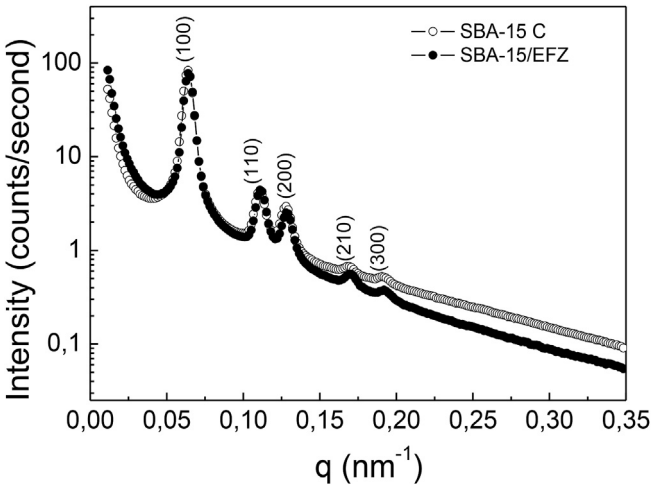

Fig. 2. Small angle X-ray scattering of ordered mesoporous silica SBA-15 sample.

3.1.2. Nitrogen sorption isotherms

Figs. 3 and 5 shows that Nitrogen adsorption isotherm for MCM-41 and SBA-15 samples are similar to those ones reported by [9] and [12], respectively. The isotherm of MCM-41 sample has not shown hysteresis loop, as can be seen (Fig. 3), the adsorption isotherm shows a distinct step in the relative pressure range from 0.3 to 0.5, which reflects the capillary condensation of N_2 in cylindrical mesopores. The sharpness of the branched adsorption is an indicative of a narrow porous size distribution (PSD) shown in Fig. 4.

The isotherm of SBA-15 samples has shown hysteresis loop with sharp adsorption and desorption branch. The sharpness of the branched adsorption is an indicative of a narrow porous size distribution (PSD) shown in Fig. 6. The branched adsorption was located at relative pressures in the 0.65–0.8 range, a high relative pressure, similarly to good-quality mesoporous materials [17,25]. The textural properties of the MCM-41 and SBA-15 samples were show in Table 1, these parameters were similars to the mesopore size for materials with honeycomb structures in good agreement with those reported by [9] for MCM-41 and [12] for SBA-15, respectively. The uniform channels and honeycomb structure characteristics of the MCM-41 and SBA-15 silica obtained were confirmed by the HRTEM image as shown in Figs. 9 and 10. The pore size and the wall thickness average obtained were 3.4 and 9.4 nm for pore size and 1.1 and 3.1 nm for wall thickness, respectively, whose results were obtained directly of image.

3.1.3. HRTEM

The HRTEM micrograph in Figs. 7 and 8 reveals that the MCM-41 and SBA-15 samples possess a mesoporous arrangement with high symmetry hexagonal.

3.1.4. Thermal analysis

DSC curves of the pure EFZ, SBA-15, physical mixture, and EFZ/SBA-15 (1:1 and 1:2) are shown in Fig. 7. DSC curve of EFZ (Fig. 9) shows a sharp endothermic peak that corresponds to melting in the temperature of 132 °C [enthalpy change (ΔH) = 45.38 J g^{-1}]. After melting, two peaks are observed due to thermal decomposition. The DSC curve of SBA-15 presents an endothermic transition occurring between 35 and 100 °C that was assigned to dehydration (unbound water). After this event it was not observed any transition indicating that this material is thermally stable up to 500 °C. It is observed also in the DSC curve of the EFZ/SBA-15 material the absence of the peak related to the melting of the EFZ at 132 °C, evidencing that there is not free EFZ, as differently is observed in

Table 1
Textural and structural parameters for the MCM-41 and SBA-15 samples.

Samples	XRD interplanar spacing $d_{(100)}$ (nm)	XRD lattice parameter a (nm)	BET surface area S_{BET} (m^2/g)	Single-point pore volume (cc/g)	α_s-plot analysis		PSD analysis		HRTEM	
					Mesopore volume (cc/g)	Micropore volume (cc/g)	Total pore volume (cc/g)	Pore size (nm)	Pore size (nm)	Wall thickness (nm)
MCM-41	3.68	4.26	892	0.91	0.91	0	0.91	3.65	3.40	0.77
MCM-41/EFZ	3.56	4.12	553	0.56	0.60	0	0.60	3.65	–	–
SBA-15	9.82	11.4	663	0.89	0.79	0.08	0.87	9.45	9.40	3.2
SBA-15/EFZ	9.82	11.4	370	0.62	0.61	0.02	0.63	9.55	–	–

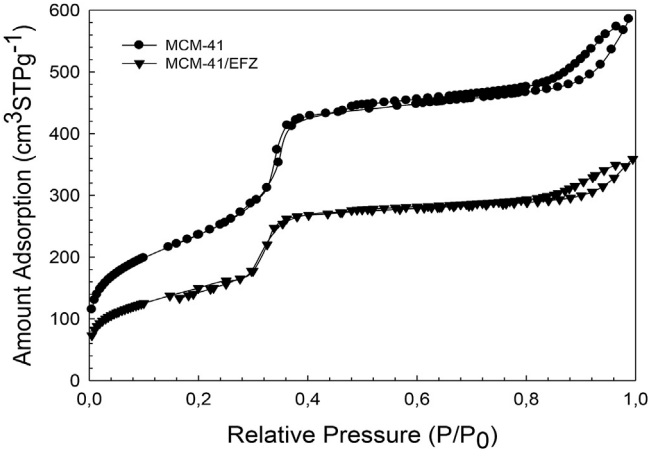

Fig. 3. N_2 sorption isotherm at 77 K for MCM-41 and MCM-41/EFZ samples.

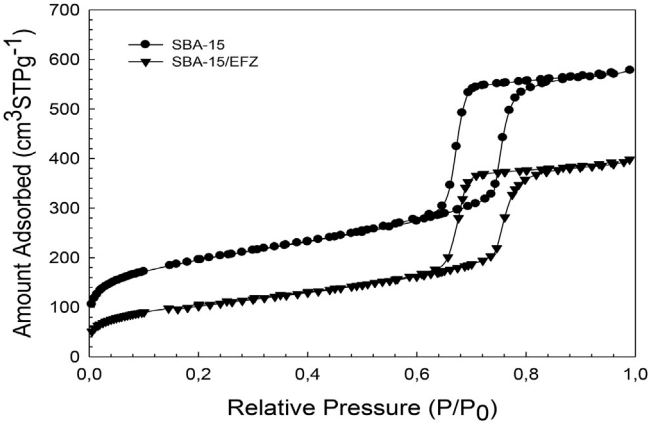

Fig. 5. N_2 sorption isotherm at 77 K for SBA-15 and SBA-15/EFZ samples.

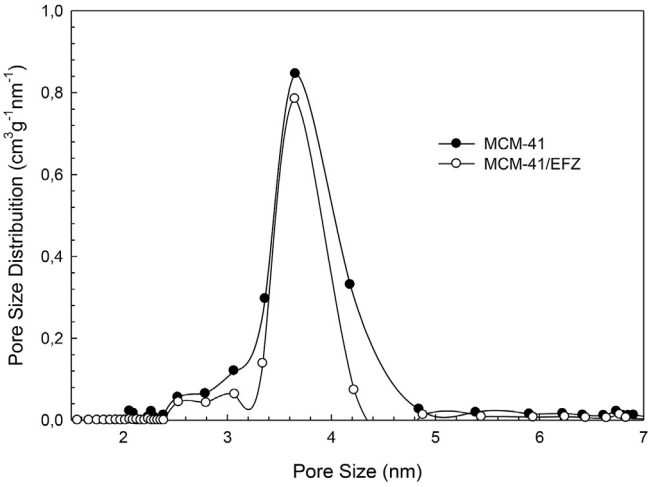

Fig. 4. Pore size distribution calculated from N_2 sorption isotherm of MCM-41 and MCM-41/EFZ samples.

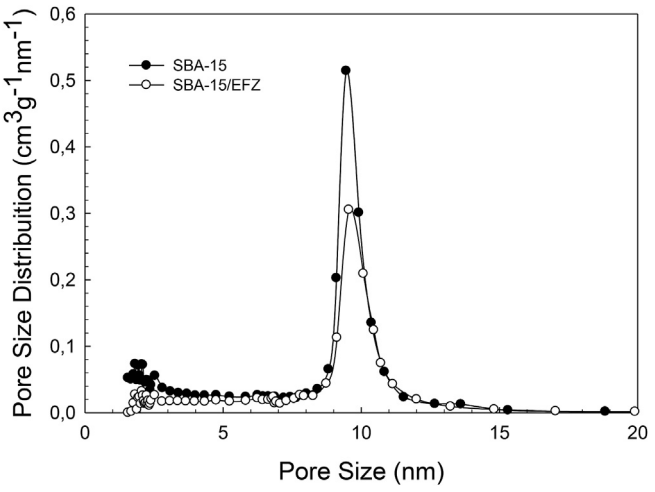

Fig. 6. Pore size distribution calculated from N_2 sorption isotherm of SBA-15 and SBA-15/EFZ samples.

DSC curve of physical mixture SBA-15/EFZ.

The thermal behavior of MCM-41 is illustrated in Fig. 10. The DSC curves of the 1:1 physical mixture of the EFZ and of MCM-41 correspond to the added signed from the pure components. The preparation contains a ratio of 1:1w:w also shows a peak at 132 °C characterizing the presence of free EFZ. However, the preparation of EFZ1:2:MCM that the drug was not incorporated.

3.2. In vitro drug release study

The release kinetics of EFZ from MCM-41 and SBA-15 were studied as a function of time and the results are shown in Fig. 11. Dissolutions were fit into various kinetic models and data are presented in Table 2. The adjusted correlation coefficient (R^2) was used as an indicator of the best fitting, for each of the models considered. Both samples have a rapid initial burst release of EFZ of

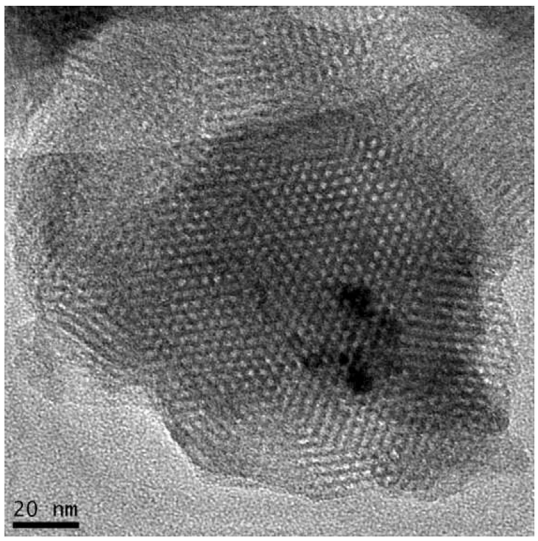

Fig. 7. Transmission electronic microscopy image of MCM-41 calcined sample.

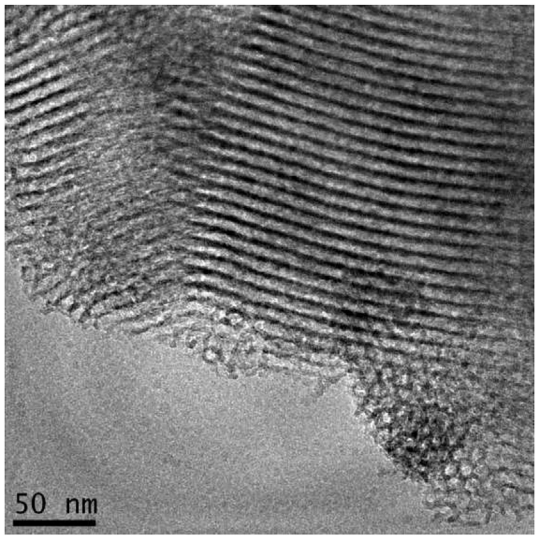

Fig. 8. Transmission electronic microscopy image of SBA-15 calcined sample.

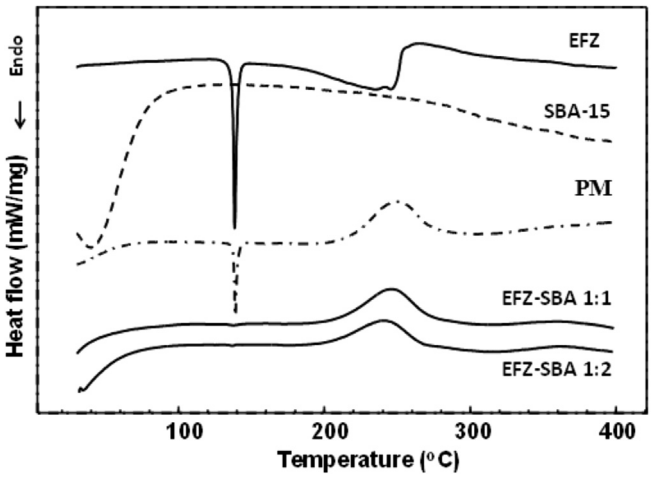

Fig. 9. DSC curves of the pure EFZ, SBA-15, physical mixture, and SBA-15/EFZ (1:1 and 1:2) recorded in dynamic nitrogen atmosphere (50 mL min^{-1}), and heating rate 10 °C min^{-1}.

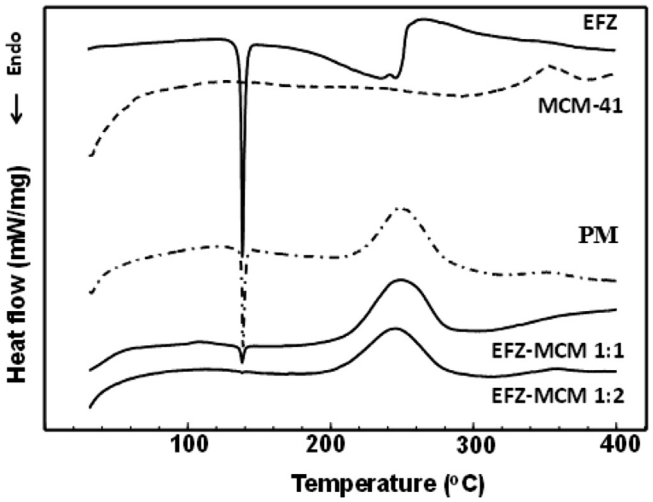

Fig. 10. DSC curves of the pure EFZ, MCM-41, physical mixture, and MCM-41/EFZ (1:1 and 1:2) recorded in dynamic nitrogen atmosphere (50 mL min^{-1}), and heating rate 10 °C min^{-1}.

approximately four to eight percent in the first ten minutes, due to fast dissolution of molecules adsorbed on surface. SBA-15/EFZ presents a faster release rate with more than 50% released in 60 min and follow a first-order pattern. A similar result was found in SBA-15 charged with gentamicin sulfate where the release profiles exhibited a pronounced initial burst release effect of 60% under one hour, followed by a very slow release pattern [26]. However, in contrast, MCM-41/EFZ has shown a slow release rate with less than 30% released after 60 min with a best fit for dissolution data modeling of a zero-order with F_0 model. Additionally, the basket speed was increased at the end of the run for a sustained period of 30 min (at 250 rpm) to force the release of remainder EFZ in silica. After the spin, the MCM-41/EFZ still retained approximately 54% of the drug compared to a modest value of 6% for SBA-15/EFZ. Therefore, these facts reveal a higher affinity of the drug for MCM-41 and the zero order release rate constant of 0.304 min^{-1} indicates that the release of EFZ can be sustained for over a period of more than 4 h. Supporting this observation, Marzouqa and co-workers describes ephedrine-loaded MCM-41 systems with a bimodal release pattern consisting of a Higuchi model in the first six hours and a slow first order release rate for over 20 h [27]. The results indicate that pore channel length, particle morphology and pore size are key parameters of the release kinetics. It was found that there are two main factors that influence the release of drugs involving drug/matrix [27,28]: In this case, the structure of porous materials (highlighting the wall thickness, specific surface area and pore size) and functional groups present on the surface of mesoporous structures, as well as, in the organic groups of the molecules of the drug used.

Regarding the effect of pore size, it is generally believed that smaller mesoporous size will affect adsorption and release of drug molecules [27,28] and, as demonstrated by the results of these studies, the material with higher size of the mesoporous, SBA-15, showed a higher release rate of EFZ and a different behavior of dynamic release compared to MCM-41, as summarizes the kinetics of drug release showed in Table 2.

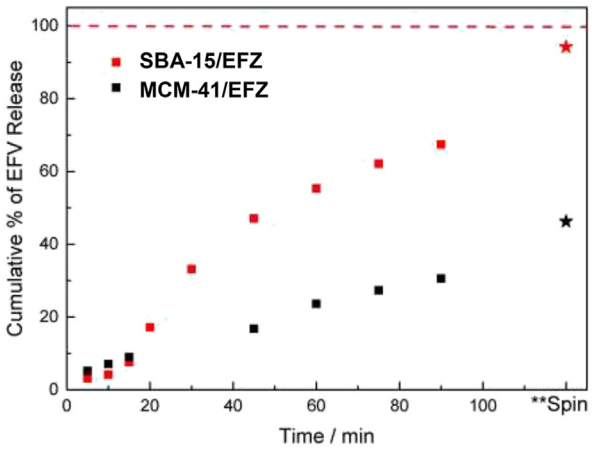

☆
** Infinity point: the basket speed was increased to 250 rpm at the end of the run (after 90 minutes) for a sustained period of 30 minutes

Fig. 11. EFZ profile of release kinetics of MCM-41 and SBA-15 versus time.

Table 2
Kinetic model fitting for the EFZ release data.

Model	Parameters	SBA-15/EFZ	MCM-41/EFZ
Zero order	K_0	0.8414	0.3658
	R_2 adjusted	0.9465	0.9312
Zero order with F0	K_0	0.8280	0.3041
	R_2 adjusted	0.9393	0.9928
	F_0	0.8047	4.0542
First order	K_1	0.0128	0.0042
	R_2 adjusted	0.9599	0.9543
Higuchi	K_H	6.3695	2.9712
	R_2 adjusted	0.8215	0.9497
Korsmeyer–Peppas	K_{KP}	0.5138	1.7348
	R_2 adusted	0.9026	0.9830
	n	1.1282	0.6280

4. Conclusions

Ordered mesoporous silicas containing encapsulated EFZ was synthetized and characterized. A narrow porous size distribution with uniformity and conserved structure was confirmed to MCM-41 and SBA-15. The smaller pore sizes of MCM-41 appears to control the EFZ release with a zero-order pattern over several hours, which is extremely important to the development of more efficient delivery systems. This approach has the potential to become the basis for the development of new drug release systems containing non-nucleoside reverse transcriptase inhibitors for anti-HIV therapies.

Acknowledgments

Thanks are due to FAPESP (LC Cides da Silva, the 2011/03072-7), the Foundation for Science and Technology of Pernambuco (FACEPE) and financial support from CNPq.

References

[1] R.P. Brettle, A. Wilson, S. Povey, S. Morris, R. Morgan, C.L.S. Leen, S. Hutchinson, S. Lewis, S. Gore, Combination therapy for HIV: the effect on inpatient activity, morbidity and mortality of a cohort of patients, Int. J. STD AIDS 9 (1998) 80–87.
[2] J. Ren, J. Milton, K.L. Weaver, S.A. Short, D.I. Stuart, D.K. Stammers, Structural basis for the resilience of efavirenz (DMP-266) to drug resistance mutations in HIV-1 reverse transcriptase, Structure 8 (2000) 1089–1094.
[3] S.D. Young, S.F. Britcher, L.O. Tran, L.S. Payne, W.C. Lumma, T.A. Lyle, J.R. Huff, P.S. Anderson, D.B. Olsen, S.S. Carroll, L-743, 726 (DMP-266): a novel, highly potent nonnucleoside inhibitor of the human immunodeficiency virus type 1 reverse transcriptase, Antimicrob. Agents Chemother. 39 (1995) 2602–2605.
[4] C.Z. Matthews, E.J. Woolf, R.S. Mazenko, H. Haddix-Wiener, C.M. Chavez-Eng, M.L. Constanzer, G.A. Doss, B.K. Matuszewski, Determination of efavirenz, a selective non-nucleoside reverse transcriptase inhibitor, in human plasma using HPLC with post-column photochemical derivatization and fluorescence detection, J. Pharm. Biomed. Anal. 28 (2002) 925–934.
[5] J.O. Adjene, J.A. Avbunudiogba, P.E. Awhin, P.S. Igbigbi, Biochemical effects of chronic administration of efavirenz on the intracranial auditory relay centers of adult Wistar rats, Genom. Med. Biomark. Health Sci. 4 (2012) 85–89.
[6] R. Langer, Selected advances in drug delivery and tissue engineering, J. Control. Release 62 (1999) 7–11.
[7] S. Al-kader Ahmed, M. Gaber, M.H. Mohamed, M.E. El-Zeiny, Nanostructure-loaded mesoporous silica for controlled release of coumarin derivatives: a novel testing of the hyperthermia effect, Eur. J. Pharm. Biopharm. 77 (2011) 66–74.
[8] I.I. Slowing, J.L. Vivero- Escoto, C.W. Wu, V.S.Y. Lin, Mesoporous silica nanoparticles as controlled release drug delivery and gene transfection carriers, Adv. Drug Deliv. Rev. 60 (2008) 1278–1288.
[9] C.T. Kresge, M.E. Leonowics, W.J. Roth, J.C. Vartuli, J.S. Beck, Ordered mesoporous molecular sieves synthesized by a liquid crystal template mechanism, Lett. Nat. 369 (1992) 710–712.
[10] J.S. Beck, J.C. Vartulli, W.J. Roth, M.E. Leonowics, C.T. Kresge, K.D. Schmidt, W. Chu, D.H. Olson, E.W. Sheppard, A new family of mesoporous molecular sieves prepared whit liquid crystal templates, J. Am. Chem. Soc. 114 (1992) 10834–10843.
[11] D. Zhao, J. Feng, Q. Huo, N. Melosh, G.F. Fredrickson, B.F. Chmelka, G.D. Stucky, Triblock copolymer syntheses of mesoporous silica with periodic 50 to 300 angstrom pores, Science 279 (1998) 548–552.
[12] D. Zhao, Q. Huo, J. Feng, B.F. Chmelka, G.D. Stucky, Nonionic triblock and star diblock copolymer and oligomeric surfactant syntheses of highly ordered, hydrothermally stable, mesoporous silica structures, J. Am. Chem. Soc. 120 (1998) 6024–6036.
[13] F. Zhang, H. Yan, Meng Yang, Y.Y. Meng, C. Yu, B. Tu, D. Zhao, Understanding effect of wall structure on the hydrothermal stability of mesostructured silica SBA-15, J. Phys. Chem. B 109 (2005) 8723–8732.
[14] A. Szegedi, M. Popova, I. Goshev, S. Klebert, J. Mihaly, Controlled drug release on amine functionalized spherical MCM-41, J. Solid State Chem. 194 (2012) 257–263.
[15] A.R. Nascimento, G. Rodrigues, J.C. Santana, A.M.G. Pedrosa, M.J.B. Souza, Catalytic esterification of oleic acid over SO^{2-}_4/MCM-41 nanostructured materials matter, Sci. Appl. 2 (2011) 706–709.
[16] N. Xiao, L. Wang, S. Liu, Y. Zou, C. Wang, Y. Ji, J. Song, F. Li, X. Meng, F.S. Xiao, High-temperature synthesis of ordered mesoporous silicas from solo-hydrocarbon surfactants and understanding of their synthetic mechanisms, J. Mater. Chem. 19 (2008) 661–665.
[17] M. Kruk, M. Jaroniec, A. Sayari, Application of large pore MCM-41 molecular sieves to improve pore size analysis using nitrogen adsorption measurements, Langmuir 13 (1997) 6267–6273.
[18] L.C. Cides da Silva, L.B.O. dos Santos, G. Abate, I.C. Cosentino, M.C.A. Fantini, J.C. Masini, J.R. Matos, Adsorption of Pb^{2+}, Cu^{2+} and Cd^{2+} in FDU-1 silica and FDU-1 silica modified with humic acid, Microporous Mesoporous Mater. 110 (2008) 250–259.
[19] FDA. Recommended Dissolution Methods – Search Results for 'efavirenz', http://www.accessdata.fda.gov/scripts/cder/dissolution/dsp_SearchResults_Dissolutions.cfm. (accessed 23.05.14).

[20] Brazilian Pharmacopoeia, fifth ed., ANVISA, Brasília, 2010, pp. 916–917.
[21] B. Singh, T. Kaur, S. Singh, Correction of raw dissolution data for loss of drug and volume during sampling, Indian J. Pharm. Sci. 59 (1997) 196.
[22] Harmon Aronson, Correction factor for dissolution profile calculations, J. Pharm. Sci. 82 (11) (1993), 1190–1190.
[23] United States Pharmacopoeia. 579. 583, 2007.
[24] Yong Zhang, et al., DDSolver: an add-in program for modeling and comparison of drug dissolution profiles, AAPS J. 12 (3) (2010) 263–271.
[25] M. Kruk, M. Jaroniec, Characterization of the porous structure of SBA-15, Chem. Mater. 12 (2000) 1961–1968.
[26] A.L. Doadrio, et al., Mesoporous SBA-15 HPLC evaluation for controlled gentamicin drug delivery, J. Control. Release 97 (1) (2004) 125–132.
[27] Dua'a M. Marzouqa, et al., Effect of particle morphology and pore size on the release kinetics of ephedrine from mesoporous MCM-41 materials, J. Porous Mater. 19 (5) (2012) 825–833.
[28] María Vallet-Regí, Francisco Balas, Daniel Arcos, Mesoporous materials for drug delivery, Angew. Chem. Int. Ed. 46 (40) (2007) 7548–7558.